Potential improvements of lung and prostate MLC tracking investigated by treatment simulations

Jakob Toftegaard[1], Paul J. Keall[2], Ricky O'Brien[2], Dan Ruan[3], Floris Ernst[4], Noriyasu Homma[5], Kei Ichiji[5], Per Rugaard Poulsen[1]

[1]Department of Oncology, Aarhus University Hospital, 8000 Aarhus C, Denmark

[2] Radiation Physics Laboratory, Sydney Medical School, University of Sydney, 2006 NSW Australia

[3]Department of Radiation Oncology, University of California, Los Angeles, California 90095

[4]Institute for Robotics and Cognitive Systems, University of Lübeck, Lübeck 23562, Germany

[5]Department of Radiological Imaging and Informatics, Tohoku University Graduate School of Medicine, Sendai 980-8579, Japan

Corresponding author:

Per Rugaard Poulsen

Aarhus University Hospital

Nr Brogade 44, 8000 Aarhus C, Denmark

Tel: +4578462651

Fax: +4578464522

Email: per.poulsen@rm.dk

Abstract

Purpose/objectives: Intrafraction tumor motion during external radiotherapy is a challenge for the treatment accuracy. A novel technique to mitigate the impact of tumor motion is real-time adaptation of the MLC aperture to the motion, also known as MLC tracking. Although MLC tracking improves the dosimetric accuracy, there are still residual errors. Here, we investigate and rank the performance of five prediction algorithms and seven improvements of an MLC tracking system by extensive tracking treatment simulations.

Materials and Methods: An in-house developed MLC tracking simulator that has been experimentally validated against an electromagnetic guided MLC tracking system was used to test the prediction algorithms and tracking system improvements. The simulator requires a Dicom treatment plan and a motion trajectory as input and outputs all motion of the accelerator during MLC tracking treatment delivery. For lung tumors, MLC tracking treatments were simulated with a low and a high modulation VMAT plan using 99 patient-measured lung tumor trajectories. For prostate, tracking was also simulated with a low and a high modulation VMAT plan, but with 695 prostate trajectories. For each simulated treatment, the tracking error was quantified as the mean MLC exposure error, which is the sum of the over-exposed area (irradiated area that should have been shielded according to the treatment plan) and the under-exposed area (shielded area that should have been irradiated).

First, MLC tracking was simulated with the current MLC tracking system without prediction, with perfect prediction (Perfect), and with the following five prediction algorithms: Linear Kalman filter (Kalman), Kernel density estimation (KDE), Linear adaptive filtering (LAF), Wavelet-based multiscale autoregression (wLMS), and Time variant seasonal autoregression (TVSAR). Next, MLC tracking was simulated using the best prediction algorithm and seven different tracking system improvements: no localization signal latency (1), doubled maximum MLC leaf speed (2), halved MLC leaf width (3), use of Y backup jaws to track motion perpendicular to the MLC leaves (4), dynamic collimator rotation for alignment of the MLC leaves with the dominant target motion direction (5), improvements 4 and 5 combined (6), and all improvements combined (7).

Results: All results are presented as the mean residual MLC exposure error compared to no tracking. In the prediction study, the residual MLC exposure error was, 47.0% (no prediction), 45.1% (Kalman), 43.8% (KDE), 43.7% (LAF), 42.1% (wLMS), 40.1% (TVSAR) and 36.5% (Perfect) for lung MLC tracking. For prostate MLC tracking. it was 66.0% (no prediction), 66.9% (Kalman) and 63.4% (Perfect) . For lung with TVSAR prediction, the residual MLC exposure error for the seven tracking system improvements was 37.2%(1), 38.3%(2), 37.4%(3), 34.2%(4), 30.6%(5), 27.7%(6), and 20.7%(7). For prostate with no prediction, the residual MLC exposure error was 61.7%(1), 61.4%(2), 55.4%(3), 57.2%(4), 47.5%(5), 43.7%(6), and 38.7%(7).

Conclusion: For prostate, MLC tracking was slightly better without prediction than with linear Kalman filter prediction. For lung, the TVSAR prediction algorithm performed best. Dynamic alignment of the collimator with the dominant motion axis was the most efficient MLC tracking improvement except for lung tracking with the low modulation VMAT plan, where jaw tracking was slightly better.

1 Introduction

Intrafractional motion limits the accuracy of current radiotherapy of moving targets[1-3]. Tumor motion blurs the delivered dose and requires enlarged margins to encompass the tumor target within the high dose volume. With the increased use of hypofractionated regimens with few high dose fractions delivered as stereotactic body radiation therapy (SBRT), it becomes critical to deliver the correct dose to a target with tight margins. Accurate high dose treatments may be obtained with real-time motion management.

Tracking is a promising real-time motion management technique where the treatment is continuously adapted to the tumor motion. Tracking is an option on two commercially available accelerators, the robotic CyberKnife[4] accelerator and the gimbal mounted Vero accelerator[5]. These systems are highly specialized and not in widespread clinical use. Two strategies for performing tracking on a conventional accelerator have been proposed. In 2001 Keall et al. proposed to shift the MLC aperture to follow the tumor motion[6] (MLC tracking) and in 2005 D'Souza et al. proposed to shift the treatment

68 couch to counteract the tumor motion[7] (Couch tracking). MLC tracking has been used clinically since 2013 based on a
69 Varian Trilogy accelerator and an in-house developed MLC tracking system[8]. Couch tracking so far is not in clinical use.
70 Although no vendors of conventional linear accelerators offer clinically approved tracking solutions, tracking is an option
71 in research mode on a TrueBeam accelerator (Varian Medical System, Palo Alto, CA).

72 The MLC tracking procedure can be divided into three steps: Real-time target localization with prediction to overcome
73 tracking system latencies, MLC leaf fitting of the MLC aperture to the predicted target position, and MLC leaf adjustment
74 to the fitted leaf positions. Although MLC tracking improves the dosimetric accuracy, there are still residual dosimetric
75 errors due to limitations of the accelerator and tracking system. These limitations can be associated with each of the three
76 tracking steps[9]. A major limitation for real-time target localization is the latency between target movement and MLC
77 adaptation. The finite width of the MLC leaves hinders exact MLC fitting to motion perpendicular to the MLC leaves. The
78 MLC leaves have a limited acceleration and speed that result in MLC adjustment errors. The overall MLC tracking
79 performance is typically dominated by the poorest performing parts in the tracking chain. Therefore, it is important to
80 identify and improve these parts. Unlike other tracking systems, the MLC perform both tracking and possibly dynamic plan
81 modulation, which might limit the capability of MLC tracking due to the limited leaf dynamics. However, MLC tracking has
82 some advantages over the other tracking techniques: It can be applied with a standard linac, it can adapt to
83 deformations[10] and rotations[11], and it is the obvious first choice for tracking on an MR-linac.

84 Tracking system improvements can be divided into software and hardware changes. Software changes could be more
85 accurate prediction algorithms, improved leaf-fitting algorithms or new methods for controlling existing hardware. For
86 example, Fast et al.[12] used the jaws to help tracking the target motion, Pommer et al.[13] and Falk et al.[14] investigated MLC
87 tracking improvements by reduced VMAT plan complexity, and Murtaza et al.[15] created prostate VMAT plans with the
88 collimator dynamically aligned to the dominant prostate motion axis to reduce motion perpendicular to the MLC leaves.
89 Hardware changes could be a faster real-time localization system or an MLC with thinner[11] or faster leaves. Software
90 changes are often cheaper and easier to implement than hardware changes, and several linac vendors have research
91 versions of their control software that allow experimental software without conflicting with the clinical software.

While experiments constitute the backbone for proof-of-principle tests and characterization of MLC tracking, experiments can only be used to investigate the current implementation of a tracking system, and this only for a relatively small dataset with limited statistical power. In contrast, realistic tracking simulations allow exploration of new tracking approaches and potential tracking system improvements not yet realized experimentally. With large-scale simulations, it is possible to obtain better statistics while focusing on one isolated parameter at a time in the tracking chain to explore its significance for the overall tracking performance. This is important in order to identify the most useful tracking system improvements prior their implementation. In this paper, we use realistic MLC tracking simultations to investigate and rank a range of potential improvements of current MLC tracking systems based on their ability to improve MLC tracking of both prostate and lung tumor motion.

2 Material and methods

In this study, we first determine the best prediction algorithm for MLC tracking (Section 2.A) and then investigate further tracking system improvements incorporating the optimal prediction algorithm (Section 2.B). For all analysis, we used an experimentally validated MLC tracking simulator[16]. The simulator emulates the behavior of Calypso electromagnetic guided MLC tracking on a TrueBeam accelerator equipped with a Millennium MLC (Varian Medical Systems)[17]. The simulator requires a Dicom treatment plan and a motion trajectory as input. It simulates all accelerator motions and MU delivery and outputs log files similar to the TrueBeam accelerator with these parameters as well as the MLC exposure error. The MLC exposure error describes the discrepancy between the actual MLC aperture and the ideal MLC aperture, which is the planned MLC aperture at the current gantry angle shifted to the current target position in beam's eye view[9]. The MLC exposure error is quantified as the sum of the under-exposed MLC area (area in beam's eye view that should receive irradiation, but is shielded by the MLC or jaws) and over-exposed MLC area (irradiated area that should be shielded)[9]. It is calculated for all three MLC tracking steps combined (localization, fitting, adjustment) by comparing the actual MLC aperture with the ideal aperture and for each of the three MLC tracking steps individually by comparing the output aperture of the step with the output aperture of the preceding step as described in Ref. 9. The MLC exposure error is used in this study as a surrogate for the dosimetric error since previous studies have shown that it correlates well with

the dose error of a given plan in terms of gamma failure rate[9,18], dose differences[15], and dose volume histogram values[15]. For each simulated treatment, the MLC exposure error was calculated for and averaged over all time points along the treatment delivery. The MLC exposure error was weighted with the dose rate or, equivalently, with the number of MU delivered at each time point in order to account for dose rate variations when calculating this surrogate for the dosimetric errors.

MLC tracking was simulated with a low and a high modulation single arc VMAT plan for prostate and lung with 358 degrees gantry rotation and the MLC leaves moving in the cranio-caudal direction[19]. The arc delivery time was 60-74s. The lung and prostate treatments were simulated with 99 lung tumor trajectories obtained with the Cyberknife Synchrony system[20] and 695 prostate trajectories captured with Calypso[21], respectively. The mean [range] of the motion range of the trajectories was 2.74mm [0.02mm-15.9mm] (LR), 7.13mm [0.15mm-42.2mm] (CC), and 3.01mm [0.14mm-13.4mm] (AP) for lung, and 0.64mm [0.26mm-4.5mm] (LR), 1.78mm [0.40mm-14.4mm] (CC), and 1.88mm [0.47mm-16.0mm] (AP) for prostate. Figure 1 shows the dominant motion direction for each trajectory, represented as the first principal component in a polar plot. Further information about the trajectories can be found in the references[20-21].

A two-sided Wilcoxon rank test was used to test for significant reductions of the mean MLC exposure error with each MLC tracking system improvement.

2.A Prediction

The accuracy of five prediction algorithms (b-f in Table 1) was investigated and compared with no prediction (a) and perfect prediction (g) for lung tumor motion. Three of the algorithms are used in existing prototype MLC tracking systems, while the two others represent state-of-the art prediction algorithms (Table 1). The linear Kalman filter prediction[17] (b) estimates the noise reduced slope of the target position and predicts the future position by linear extrapolation with the estimated slope. It only requires a few samples to start predicting, and it generally overestimates the amplitude of respiratory target motion.

Algorithms (c-f) use training data for prediction. The kernel density estimation (KDE) predictor[22] (c) estimates the target position as a weighted linear combination of the observed positions in the training data set. Each weight factor is

calculated from the similarity between an input vector consisting of the last observed target positions and the training data. KDE usually predicts well if the training data are representative of the predicted target position, but if the patient for example breathes deeper than observed in the training data, training data with this behavior must be acquired before the algorithm can perform a proper prediction.

The linear adaptive filtering (LAF) predictor[23] (d) first performs a low pass filtering of the training data. The prediction is performed by creating an input vector based on the last observed target positions and finding the position in the training data that minimizes the sum of squared distances between the input vector and the training data.

The wavelet-based multiscale auto regression (wLMS) predictor[24] (e) performs an à trous wavelet decomposition of the input signal. The predicted position is found with the assumption of a fixed periodicity of the wavelets, albeit different for each decomposition scale. The weights for each wavelet are found by least-squares fitting of a part of the incoming signal's history, again individual for each scale.

The time-variant seasonal autoregressive (TVSAR) predictor[25] (f) is based on a seasonal autoregressive method (SAR), which assumes oscillating target position with a fixed period. It predicts the position based on the position at the same phase of the previous oscillations. TVSAR extends the SAR method with a time variant correction for fluctuations in the period by estimating the current phase and the corresponding time position of this phase in the previous periods. Moreover, the residuals from the predicted oscillating components are adaptively compensated by using a normal autoregressive model.

During MLC tracking, the TrueBeam accelerator predicts a new target position every 10ms based on the latest Calypso position measurements. The simulations assumed a fixed Calypso measurement rate of 25Hz and a fixed time interval T_{Signal}= 54ms from measurement to arrival of the measured position into the tracking system[16]. T_{Signal} = 54ms corresponds to the mean value found in a series of TrueBeam tracking experiments[17]. Furthermore, the position predictions every 10ms were assumed to occur 5ms, 15ms, 25ms, and 35ms after arrival of the Calypso measurements.

In order to determine the optimal prediction lengths for a perfect prediction algorithm, MLC tracking of a circular MLC aperture was simulated with a sinusoidal target motion with 15mm peak-to-peak amplitude and 4s period. A perfect

prediction algorithm was used that looked up the target position in the trajectory a user defined time step forward. This time step was adjusted until the phase difference between the sinusoidal target motion and MLC aperture motion was zero. The prediction lengths found by this method were 106ms, 116ms, 126ms, and 136ms depending on the age of the latest arrived Calypso measurement (i.e. 5ms, 15ms, 25ms, and 35ms after position arrival). These prediction lengths were therefore used for prediction algorithms (c)-(f). However, for the linear Kalman filter, shorter prediction lengths of 86ms, 96ms, 106ms 116ms were used, since these values are used by the current Truebeam MLC tracking system with the linear Kalman filter[16]. Use of the shorter prediction lengths compensates to some degree for the tendency of the linear Kalman filter to overestimate the amplitude of respiratory motion.

It should be noted that the applied prediction lengths are shorter than the time lag of 146ms between sinusoidal target motion and MLC aperture motion found in previous MLC tracking experiments when no prediction was applied[17]. These experiments showed that a prediction length of 146ms should be used if the tracking system only predicted the target position once every 40ms immediately after receiving a new Calypso measurement. However, a shorter prediction length should be used when the target position is predicted every 10ms because the waiting time between position signals is smaller and because the MLC adjustments are smaller[26-27].

To evaluate the prediction algorithms, each trajectory was adjusted to position zero at the start of the trajectory, and VMAT MLC tracking treatments starting 60s into the trajectory were simulated. At each time point, the preceding 20s motion was used as training data for prediction algorithms (c)-(f). Lung treatments were simulated with all prediction algorithms. The accuracy of each prediction algorithm was quantified as the 3D root mean square (RMS) difference between the real-time predicted position and the actual future target position after the optimal prediction length (106ms, 116ms ,126ms, and 136ms) during each simulated treatment. Furthermore, the impact of the prediction on the MLC tracking accuracy was quantified as the mean MLC exposure error for each simulated treatment.

Prostate motion is mainly driven by effects likes bladder filling and rectal filling without the periodicity of respiration. Therefore, no prediction was used in the first clinical trial of MLC tracking of prostate cancer[8] performed with the Trilogy based research MLC tracking system. On the other hand, the Varian TrueBeam MLC tracking system uses the linear

Kalman filter as the default option. For these reasons, prostate treatments were simulated with no prediction (a), with linear Kalman filter prediction (b) and with perfect prediction (g), but not with the prediction algorithms (c)-(f) that assume periodic motion. Similar to lung, the 3D RMS prediction error and the mean MLC exposure error were calculated for each simulated prostate treatment.

To enable stratification of the results according to motion magnitude, the motion trajectory during each simulated treatment was transformed to its principal component coordinate system and the motion range along the first principal component was determined.

2.B Tracking system design improvements

The best performing prediction algorithm from the preceding section was used in a simulation study to investigate and rank potential MLC tracking system improvements . As summarized in Table 2 and described more detailed below, simulations were performed for five individual MLC tracking system improvements and two combinations hereof, i.e. seven improvements in total. While these improvements could all be investigated and compared using the same set of VMAT plans, other strategies for improved tracking that require replanning (e.g. reduced VMAT plan complexity[13-14]) were not included in this study.

The first improvement (No localization latency (1)) assumed that the Calypso position signals reach the tracking system instantaneously after the localization instead of the current mean delay of T_{Signal} = 54ms[16]. While zero localization latency is unrealistic, it was chosen here to investigate the maximal impact of latency reduction. The simulated tracking system still has residual latencies from the waiting time between localization signals and time used for leaf fitting and leaf adjustment. The shorter latency reduces the required prediction length and thereby the real-time localization errors.

The second improvement (Fast MLC (2)) emulated the effect of faster MLC leaves by multiplying the current maximum speed, acceleration, and de-acceleration of the MLC leaves[16] with a factor of two. As an example, the maximum leaf speed was increased from 2.5 cm/s to 5.0 cm/s. This improvement reduces the MLC adjustment errors.

Improvements (3)-(6) all aimed at better MLC fitting to motion perpendicular to the MLC leaves as summarized in Figure 2 and described in the following. Improvement (3) used an MLC with 2.5 mm leaf width instead of the 5 mm of the Millennium MLC. The simulations used an MLC with 2.5mm width for all leaves unlike the Varian HD-MLC, which has 32 leaf pairs of 2.5 mm width at the center and 14 leaf pairs of 5mm width on each side.

Improvement (4) used jaw tracking as implemented by Fast et al. for an MLC tracking system based on an Elekta Agility accelerator[12]. Jaw tracking reduces the leaf fitting error by opening the leaves adjacent to the MLC aperture and placing the Y-jaws at the MLC aperture border (Figure 2). The Y-jaws follow the target motion perpendicular to the MLC, which eliminates leaf-fitting errors from the first and last leaf pair in the MLC aperture.

Improvement (5) used dynamic rotation of the collimator during the VMAT treatment to reduce target motion perpendicular to the MLC leaves as proposed by Murtaza et al. for prostate MLC tracking[15]. The collimator was aligned with its leaves parallel with a dominant tumor motion direction. The collimator rotation θ was calculated by Equations (1) and (2).

$$\begin{pmatrix} x_p \\ y_p \\ z_p \end{pmatrix} = \begin{pmatrix} \cos\emptyset & 0 & -\sin\emptyset \\ 0 & 1 & 0 \\ \sin\emptyset & 0 & \cos\emptyset \end{pmatrix} \cdot \begin{pmatrix} x \\ y \\ z \end{pmatrix} \quad (1)$$

$$\theta = \tan^{-1}\frac{x_p}{y_p} \quad (2)$$

Here, (x, y, z) and (x_p, y_p, z_p) are the dominant tumor motion direction in IEC 61217 patient coordinates and in beam eye view, respectively, and $\emptyset$ is the gantry angle. Since all VMAT fields were coplanar, no transformation was needed to account for couch rotation.

For lung tumors, the first principal component of the first minute of each trajectory was used as a patient-specific dominant motion direction. For prostate, a patient-specific dominant motion direction may not be detectable from an arbitrary trajectory with possible very small motion, but a common motion direction for all patients can be used instead[15,30]. The common population-based prostate motion direction was found as the first principal component of a trajectory obtained by concatenating the first minute of the 695 prostate motion trajectories[15]. The dominant motion directions for all trajectories are shown in Figure 1.

A variance analysis was performed for both lung and prostate to quantify the fraction of motion (variance) that occurred along the dominant motion direction (i.e. along the MLC leaves) during the simulated treatments with dynamic collimator rotation. The analysis was conducted by transforming the motion trajectory to the principal component coordinate system and calculating the fraction of motion variance along the first principal component:

$$\mathbf{var}_{PC1} = \frac{var(\mathbf{T_1})}{var(\mathbf{T_1})+var(\mathbf{T_2})+var(\mathbf{T_3})} \quad (3)$$

Here, T_1 is calculated from Equation (1) while T_2 and T_3 denote motion along axes orthogonal to the dominant motion axis.

Jaw tracking (4) and dynamic collimator rotation (5) are software improvements that use the existing MLC tracking equipment. It is obvious to combine them, which was done as improvement (6). Finally, improvement (7) consisted of all improvements (1)-(5) combined.

The impact of each MLC tracking system improvement was investigated by simulating MLC tracking treatments with the low and high modulation VMAT plans and the lung tumor and prostate motion trajectories. For lung, the simulated treatments started 9 minutes (instead of 1 minute) into the trajectory to obtain larger temporal separation between determination of the dominant motion direction for the dynamic collimator rotation improvement (5) and the actual

248 treatment. However, for four trajectories a waiting time of only 4 minutes was used because the trajectories were shorter
249 than the required 10 minutes.

250 For each simulated treatment, the mean MLC exposure error was calculated for the individual steps of real-time target
251 localization, leaf-fitting, and leaf/jaw-adjustment, and for all three steps combined[9].

252 Results

253 3.A Prediction

254 Figure 3 shows the actual lung tumor position and the predicted position of the five prediction algorithms for an
255 illustrative time interval of two breathing cycles. As seen, the linear Kalman filter prediction overshot at the extrema,
256 while KDE predicted the end of the second exhale phase too early because this exhale phase was longer than in the
257 previous cycles. The three other algorithms were quite accurate with TVSAR being most accurate.

258 The mean RMS prediction error and MLC exposure error for all trajectories are shown in Figure 4 (lung) and Figure 5
259 (prostate) in order of increasing prediction error. The MLC exposure error is presented as the mean residual MLC exposure
260 error compared to no tracking, i.e. 0% means perfect tracking and 100% means no improvement over non-tracking
261 treatments.

262 For lung tumor motion, all prediction algorithms performed better than the use of no prediction (Figure 4). TVSAR had the
263 lowest prediction errors and MLC exposure errors. Averaged over both VMAT plans the mean residual MLC exposure error
264 was 36.5% (Perfect), 40.1% (TVSAR), 42.1% (wLMS), 43.7% (LAF), 43.8% (KDE), 45.1% (Kalman) and 46.8% (No prediction).
265 For perfect prediction, the residual MLC exposure error is the error caused by leaf fitting and leaf adjustment. It is worth
266 noticing that the ordering of localization errors was not directly translatable to the MLC exposure error. As an example,
267 wLMS and LAF had larger localization errors than KDE for intermediate lung tumor motion (5-10mm motion range), but
268 smaller MLC exposure errors. Small oscillations were observed for the wLMS and LAF algorithms, which increased the
269 localization error, but since the MLC cannot adapt to these fast oscillations they did not increase the MLC exposure errors.

Compared to the current linear Kalman filter prediction, the mean residual MLC exposure error was significantly reduced by LAF ($p=0.001$), KDE ($p=0.005$), wLMS ($p < 0.001$), and TVSAR ($p < 0.001$) prediction.

For prostate motion, use of no prediction resulted in more accurate target localization than the linear Kalman filter prediction, which is the default prediction for TrueBeam MLC tracking (Figure 5, left). The mean residual MLC exposure error was significantly smaller without prediction (66.0%) than with the linear Kalman filter prediction (66.9%) ($p < 0.001$), but larger than perfect prediction (63.4 %). The MLC exposure error was, however, nearly identical with and without prediction because the MLC exposure error for prostate MLC tracking is governed by MLC fitting errors rather than real-time localization errors.

While both lung and prostate prediction errors clearly increased with motion magnitude (Figures 4-5, left), the reported residual MLC exposure errors decreased with motion magnitude (Figure 4-5, right). This is because the MLC exposure error is reported relative to the error without MLC tracking. Large target motion results in large MLC exposure errors without MLC tracking and therefore relatively large exposure error reductions with MLC tracking.

3.B Tracking system design improvements

Figure 6 presents an illustrative example from a prostate treatment simulation with three of the improvements and the current tracking system. The target offset perpendicular to the MLC leaves was much smaller with the dynamic collimator rotation (Figure 6.a), and this translated directly into smaller MLC exposure error for the leaf fitting step (Figure 6.b) and for the entire MLC tracking chain (Figure 6.c). For the half leaf width MLC, the leaf-fitting MLC exposure error decreased abruptly to zero after 19 seconds as the perpendicular target offset reached 2.5mm (Figure 6.b), whereas the MLC exposure error continued to increase for the original 5mm leaf width MLC. Jaw tracking reduced the leaf fitting MLC exposure error to a high degree during most of the treatment as it eliminated fitting errors at the extreme boundaries of the MLC aperture. Comparing Figure 6.b and 6.c shows that some of the gain by improved MLC fitting was lost to extra leaf-adjustment at the end, in particular for the half leaf width MLC.

Figure 7 shows the mean residual MLC exposure error as compared to no tracking for all improvements and without other improvements than the optimal prediction strategy (TVSAR for lung , no prediction for prostate). For prostate, the total

mean residual MLC exposure error compared with no tracking was 61.7% (1), 61.4% (2), 55.4% (3), 57.2% (4), 47.5% (5), 43.7% (6) and 38.7% (7) when averaged over both VMAT plans. For lung, it was considerably smaller: 37.2% (1), 38.3% (2), 37.4% (3), 34.2% (4), 30.6% (5), 27.7% (6) and 20.7% (7). Not surprisingly, combining all the improvements reduced the MLC exposure error the most.

Looking at the individual improvements (1)-(5), dynamic collimator rotation (5) had the smallest residual MLC exposure error for prostate treatments and for lung treatments with the high modulation VMAT plan. For the low modulation lung VMAT plan, jaw tracking (4) performed slightly better. Half MLC leaf width (3) reduced the MLC exposure error to a high degree for prostate, but only slightly for lung because the improved MLC fitting came at a cost of more leaf adjustment errors. For prostate, the MLC exposure improvement was largest for large motion.

Figure 8 shows the mean MLC exposure error reduction for each of the three MLC tracking steps (target localization, leaf fitting, leaf adjustment) and for the total error. The figure shows the MLC exposure error reduction relative to the current MLC tracking system without other improvements than the optimal prediction strategy. Negative values indicate increased MLC exposure error of the MLC tracking step. Not surprisingly, no localization latency (1) reduced the target localization error due to shorter prediction lengths, but for lung tumor motion it also reduced the leaf adjustment errors because it lead to fewer extreme excursions that the MLC had to adjust to. Jaw tracking and half leaf width substantially reduced the leaf fitting errors, but they also increased the leaf adjustment errors, especially for lung treatments. On the other hand, dynamic collimator rotation improved both MLC fitting and leaf adjustment.

For the lung tumor trajectories, 83% of the motion (variance) occurred along the dominant tumor motion direction, i.e. parallel to the MLC leaves for treatments with dynamic collimator rotation, while the remaining 17% was either perpendicular to the MLC leaves or in-depth along the beam axis. For prostate, 60% of the motion variance was along the dominant motion direction.

All tracking system improvements significantly reduced the mean MLC exposure error relative to the current system with optimized prediction ($p < 0.01$).

Discussion

In this study, large-scale MLC tracking simulations were used to investigate and rank the MLC tracking accuracy of several prediction algorithms and potential MLC tracking system improvements. The best localization accuracy was obtained without prediction for prostate motion and with the TVSAR prediction algorithm for lung tumor motion. Software improvements of the MLC tracking system by dynamic collimator rotation or jaw assisted MLC tracking were more efficient than the probably more expensive hardware improvements of a faster localization system or an MLC with faster or thinner leaves. The analysis of MLC exposure errors for each of the three steps in the tracking chain (Figure 8) gave valuable insight into the particular characteristics of each MLC tracking system improvement. As an example, some of the improvements in the MLC fitting step gained by thinner MLC leaves or jaw tracking was shown to be lost in the leaf adjustment step due to more motion required by the leaves or jaws.

Prostate motion prediction was only investigated with the linear Kalman filter and not with prediction algorithms that rely on semi-periodic motion. The lung motion prediction study included a wider range of prediction algorithm performances than in previous comparative studies of prediction algorithms[29,31]. The study is to our best knowledge the first investigation of the impact of the prediction algorithm on the MLC tracking accuracy. Large prediction error reduction by the best algorithms only lead to quite modest reductions in the MLC tracking error (Figures 4-5) because the tracking error was governed by other links in the MLC tracking chain than target localization. A limitation of the prediction part of the study was that the prediction algorithms were only investigated for the specific conditions used in the MLC tracking simulations, i.e. only for the prediction lengths required for the Varian TrueBeam tracking system and with the assumption of temporally equally spaced position signals measured without noise. The relative ranking of the algorithms might change for other prediction lengths or more realistic position sample modeling with varying sampling rates and measurement noise. Furthermore, the investigated algorithms are only a subset of existing prediction algorithms, and there might be algorithms that are more accurate. Different techniques can be applied to improve the presented algorithms: Individual prediction algorithm parameters could be optimization based on a trajectory acquired before treatment start, prediction could be performed simultaneously for all three coordinates[32], and several prediction algorithms could be run in parallel with real-time selection of the best performing algorithm for the actual motion[33].

Prostate MLC tracking was only very modestly affected by the improved target localization of no localization latency or the improved MLC adjustment of faster MLC leaves (Figure 7). Improved MLC fitting by thinner MLC leaves, jaw tracking or dynamic collimator rotation had a much larger impact because MLC exposure errors for prostate mainly arise from the limited MLC fitting to persistent target offsets perpendicular to the MLC leaves[17]. The MLC exposure error reduction by dynamic collimator rotation was about twice the reduction by thinner MLC leaves or jaw tracking (Figure 8, lower). Unlike prostate tracking, lung MLC tracking was affected by improvements in all three parts of the MLC tracking chain. For the high modulation lung VMAT plan, no localization latency, faster MLC leaves, thinner MLC leaves and jaw tracking gave similar MLC exposure error reductions, while dynamic collimator rotation gave 4-5 times larger reductions (Figure 8, upper right). For the low modulation lung VMAT plan, jaw tracking was much more efficient and outperformed dynamic collimator rotation because the jaws formed a larger part of the MLC aperture and therefore could eliminate a larger fraction of the MLC fitting errors (Figure 8, upper left).

Thinner MLC leaves improved leaf fitting to a high degree for both tumor sites, but it also increased leaf motion and therefore leaf adjustment errors. The added leaf motion was only minor for prostate due to small target motions while it was much larger for the respiratory moving lung targets, leading to only a minor total improvement (Figure 8). Pommer et al.[13] experimentally compared MLC tracking with a Millennium MLC and HDMLC for prostate and found better MLC tracking with thinner MLC leaves in good agreement with these results. The same study also found larger MLC exposure errors for more modulated VMAT plans[13], which is also what we observed when comparing high and low modulation VMAT plans. Besides improved MLC fitting, thinner MLC leaves may also allow VMAT planning with more conformal dose distributions to the tumor shape. This advantage of thinner MLC leaves was not investigated in the current study. Furthermore, the study only investigated MLC fitting to a pre-defined MLC aperture generated during planning for a 5mm leaf width MLC. Fitting directly to an ideal fluence would be more in favor of thin MLC leaves than the current study.

The effect of jaw tracking is directly related to the plan complexity since only MLC fitting errors at the edge of the MLC aperture are eliminated (Figure 2(4)). For this reason, jaw tracking was particularly good for the low modulation lung VMAT plan, which was almost conformal with very little modulation. The improvements were much smaller for the high modulation lung and prostate plans, but also for the low modulation prostate plan because it had leaf pairs at the edges

368 that opened and closed during the VMAT delivery, which made jaw tracking inefficient. The ranking of the jaw tracking
369 strategy relative to the other tracking system improvements may change if other VMAT plans were studied.

370 The simulations of MLC tracking with dynamic collimator rotation used the same MLC apertures as function of gantry
371 angle as in the original static collimator VMAT plans. While this naturally will give distorted 3D dose distributions, the use
372 of unchanged aperture shapes allowed direct comparison of the MLC exposure errors between all tracking system
373 improvements in the study. In a recent simulation study for prostate cancer, Murtaza et al. demonstrated that dynamic
374 collimator rotation VMAT plans can be generated with the same plan quality as clinically applied static collimator plans,
375 but with significantly reduced MLC tracking errors[14]. A limitation of the dynamic collimator rotation is that the dominant
376 tumor motion direction must be known at the time of treatment planning. For prostate, both the current study and the
377 study by Murtaza et al.[15] showed that a population-based tumor motion direction is sufficient. For lung tumors, the
378 simulations in this study used a motion direction recorded 10 minutes before the actual treatment simulation, which is not
379 feasible in a clinical workflow. Instead, a 4DCT scan can be used to find the dominant motion axis. Worm et al.[34] found for
380 liver SBRT that the motion directionally in the planning 4DCT was stable throughout the SBRT treatment course. A
381 limitation of the dynamic collimator approach is that the collimator angle becomes a function of the gantry angle,
382 whereby the degree of freedom in selecting the collimator angle during treatment planning is lost. Although this was
383 shown not to degrade the plan quality for prostate VMAT[15] it may be a more serious limitation for more complex VMAT
384 planning.

385 A limitation of this study was the small number of investigated treatment plans. The treatment plans have previously been
386 used to investigate the performance of different MLC tracking systems[9,19,35,36]. They were designed to span the range of
387 clinical complexity with the low modulation plans being nearly conformal arc plans and the high modulation plans being
388 considerably more complex with 1.75 times as many MU as the low modulation plans.

389 The two combined MLC tracking improvements (6) and (7) reduced the mean MLC exposure error more than any of the
390 individual improvements, thereby demonstrating the added value of several MLC tracking system improvements. The
391 combination of dynamic collimator rotation and jaw tracking was almost as good as all combinations combined, and it may

be the most obvious improvement to implement since it only requires changes in the treatment planning and accelerator software. Dynamic collimator rotation VMAT can be performed in research mode on a Varian TrueBeam accelerator while Fast et al. have implemented jaw tracking on an Elekta Agility accelerator[12].

Conclusion

The performance of five prediction algorithms and no prediction for MLC tracking were extensively investigated with an experimentally validated tracking simulator. For lung MLC tracking, the TVSAR prediction algorithm performed best. For prostate MLC tracking, no prediction was slightly better than a linear Kalman filter prediction.

Seven strategies for improving MLC tracking were tested with the simulator. All strategies reduced the mean MLC exposure error compared with the current implementation. Dynamic alignment of the collimator with the dominant motion axis resulted in the largest improvement on average, while using the backup jaws to track motion perpendicular to the MLC leaves led to the largest improvements for the low modulation lung plan.

Acknowledgement

This work was supported by The Danish Cancer Society, CIRRO-The Lundbeck Foundation Center for Interventional Research in Radiation Oncology, and Varian Medical Systems, Inc., Palo Alto, CA. The authors gratefully thank Drs Katja Langen and Patrick Kupelian for the prostate trajectories recorded at MD Anderson Cancer Center Orlando and Drs Yelin Suh and Sonja Dieterich for the lung tumor trajectories recorded at Georgetown University.

Conflict of interest

This project received financial support from Varian Medical Systems, Inc., Palo Alto.

References

1 P.J. Keall, G.S. Mageras, J.M. Balter, R.S. Emery, K.M. Forster, S.B. Jiang, J.M. Kapatoes, D. a Low, M.J. Murphy, B.R. Murray, C.R. Ramsey, M.B. Van Herk, S.S. Vedam, J.W. Wong, and E. Yorke, "The management of respiratory motion in radiation oncology report of AAPM Task Group 76.," Med. Phys. 33(10), 3874–3900 (2006).

2 K.M. Langen and D.T. Jones, "Organ motion and its management.," Int. J. Radiat. Oncol. Biol. Phys. 50(1), 265–78 (2001).

3 H. Shirato, Y. Seppenwoolde, K. Kitamura, R. Onimura, and S. Shimizu, "Intrafractional tumor motion: lung and liver.," Semin. Radiat. Oncol. 14(1), 10–8 (2004).

4 A. Schweikard, G. Glosser, M. Bodduluri, M.J. Murphy, and J.R. Adler, "Robotic motion compensation for respiratory movement during radiosurgery.," Comput. Aided Surg. 5(4), 263–77 (2000).

5 Y. Kamino, K. Takayama, M. Kokubo, Y. Narita, E. Hirai, N. Kawawda, T. Mizowaki, Y. Nagata, T. Nishidai, and M. Hiraoka, "Development of a four-dimensional image-guided radiotherapy system with a gimbaled X-ray head.," Int. J. Radiat. Oncol. Biol. Phys. 66(1), 271–8 (2006).

6 P.J. Keall, V.R. Kini, S.S. Vedam, and R. Mohan, "Motion adaptive x-ray therapy: a feasibility study.," Phys. Med. Biol. 46(1), 1–10 (2001).

7 W.D. D'Souza, S. a Naqvi, and C.X. Yu, "Real-time intra-fraction-motion tracking using the treatment couch: a feasibility study.," Phys. Med. Biol. 50(17), 4021–33 (2005).

8 P.J. Keall, E. Colvill, R. O'Brien, J.A. Ng, P.R. Poulsen, T. Eade, A. Kneebone, and J.T. Booth, "The first clinical implementation of electromagnetic transponder-guided MLC tracking," Med. Phys. 41(2), 20702 (2014).

9 P.R. Poulsen, W. Fledelius, B. Cho, and P. Keall, "Image-based dynamic multileaf collimator tracking of moving targets during intensity-modulated arc therapy.," Int. J. Radiat. Oncol. Biol. Phys. 83(2), e265-71 (2012).

10 Y. Ge, R.T. O'Brien, C.-C. Shieh, J.T. Booth, and P.J. Keall, "Toward the development of intrafraction tumor deformation tracking using a dynamic multi-leaf collimator.," Med. Phys. 41(2014), 61703 (2014).

11 J. Wu, D. Ruan, B. Cho, A. Sawant, J. Petersen, L.J. Newell, H. Cattell, and P.J. Keall, "Electromagnetic detection and real-time DMLC adaptation to target rotation during radiotherapy," Int. J. Radiat. Oncol. Biol. Phys. 82(3), e545–e553 (2012).

12 M.F. Fast, S. Nill, J.L. Bedford, and U. Oelfke, "Dynamic tumor tracking using the Elekta Agility MLC," Med. Phys. 41(11), 111719 (2014).

13 T. Pommer, M. Falk, P.R. Poulsen, P.J. Keall, R.T. O'Brien, and P. Munck af Rosenschöld, "The impact of leaf width and plan complexity on DMLC tracking of prostate intensity modulated arc therapy.," Med. Phys. 40(11), 111717 (2013).

14 M. Falk, T. Larsson, P. Keall, B. Cho, M. Aznar, S. Korreman, P. Poulsen, and P. Munck af Rosenschöld. The dosimetric impact of inversely optimized arc radiotherapy plan modulation for real-time dynamic MLC tracking delivery. Med. Phys. 39, 1588-94 (2012).

15 G. Murtaza, J. Toftegaard, E.U. Khan, and P.R. Poulsen, "Volumetric modulated arc therapy with dynamic collimator rotation for improved multileaf collimator tracking of the prostate," Radiother. Oncol. 122(1), 109–115 (2017).

16 J. Toftegaard, R. Hansen, T. Ravkilde, K. Macek, and P.R. Poulsen, "An experimentally validated couch and MLC tracking simulator used to investigate hybrid couch-MLC tracking," Med. Phys. 44, 798-809 (2017).

17 R. Hansen, T. Ravkilde, E.S. Worm, J. Toftegaard, C. Grau, K. Macek, and P.R. Poulsen, "Electromagnetic guided couch and multileaf collimator tracking on a TrueBeam accelerator," Med. Phys. 43(5), 2387–2398 (2016).

18 T. Ravkilde, P.J. Keall, C. Grau, M. Høyer, and P.R. Poulsen, "Time-resolved dose distributions to moving targets during volumetric modulated arc therapy with and without dynamic MLC tracking.," Med. Phys. 40(11), 111723 (2013).

19 P.J. Keall, A. Sawant, B. Cho, D. Ruan, J. Wu, P. Poulsen, J. Petersen, L.J. Newell, H. Cattell, and S. Korreman, "Electromagnetic-guided dynamic multileaf collimator tracking enables motion management for intensity-modulated arc therapy.," Int. J. Radiat. Oncol. Biol. Phys. 79(1), 312–20 (2011).

20 Y. Suh, S. Dieterich, B. Cho, and P.J. Keall, “An analysis of thoracic and abdominal tumour motion for stereotactic body radiotherapy patients.,” Phys. Med. Biol. 53(13), 3623–40 (2008).

21 K.M. Langen, T.R. Willoughby, S.L. Meeks, A. Santhanam, A. Cunningham, L. Levine, and P. a Kupelian, “Observations on real-time prostate gland motion using electromagnetic tracking.,” Int. J. Radiat. Oncol. Biol. Phys. 71(4), 1084–90 (2008).

22 D. Ruan, “Kernel density estimation-based real-time prediction for respiratory motion.,” Phys. Med. Biol. 55(5), 1311–1326 (2010).

23 V. Srivastava, P. Keall, A. Sawant, and Y. Suh, “TU-C-M100J-06: Accurate Prediction of Intra-Fraction Motion Using a Modified Linear Adaptive Filter,” Med. Phys. 34(6), 2546 (2007).

24 F. Ernst, A. Schlaefer, and A. Schweikard, “Prediction of respiratory motion with wavelet-based multiscale autoregression.,” Med. Image Comput. Comput. Assist. Interv. 10(Pt 2), 668–75 (2007).

25 K. Ichiji, N. Homma, M. Sakai, Y. Takai, Y. Narita, M. Abe, N. Sugita, and M. Yoshizawa, “Respiratory motion prediction for tumor following radiotherapy by using time-variant seasonal autoregressive techniques,” Proc. Annu. Int. Conf. IEEE Eng. Med. Biol. Soc. EMBS 6028–6031 (2012).

26 P.R. Poulsen, B. Cho, A. Sawant, D. Ruan, and P.J. Keall, “Detailed analysis of latencies in image-based dynamic MLC tracking,” Med. Phys. 37(9), 4998-5005 (2010).

27 W. Fledelius, P.J. Keall, B. Cho, X. Yang, D. Morf, S. Scheib, and P.R. Poulsen, “Tracking latency in image-based dynamic MLC tracking with direct image access.,” Acta Oncol. 50(6), 952–959 (2011).

28 J.T. Booth, V. Caillet, N. Hardcastle, R. O’Brien, K. Szymura, C. Crasta, B. Harris, C. Haddad, T. Eade, and P.J. Keall, “The first patient treatment of electromagnetic-guided real time adaptive radiotherapy using MLC tracking for lung SABR”, Radiother Oncol 121, 19–25 (2016).

29 F. Ernst, R. Dürichen, A. Schlaefer and A. Schweikard. “Evaluating and comparing algorithms for respiratory motion prediction”, Phys. Med. Biol. 58, 3911-3929 (2013).

30 P.R. Poulsen, B. Cho, K. Langen, P. Kupelian, and P.J. Keall. “Three-dimensional prostate position estimation with a single x-ray imager utilizing the spatial probability density”, Phys. Med. Biol. 53, 4331-4353 (2008).

31 A. Krauss, S, Nill, and U. Oelfke. “The comparative performance of four respiratory motion predictors for real-time tumour tracking”, Phys. Med. Biol. 56, 5303-5317 (2011).

32 D. Ruan and P. Keall, “Online prediction of respiratory motion: multidimensional processing with low-dimensional feature learning.,” Phys. Med. Biol. 55(11), 3011–25 (2010).

33 D. Moore and A. Sawant, “TH-AB-303-03: Real-Time Error Estimation for Real-Time Motion Prediction,” Med. Phys. 42(6), 3711–3711 (2015).

34 E.S. Worm, M. Høyer, W. Fledelius, A.T. Hansen, and P.R. Poulsen, “Variations in magnitude and directionality of respiratory target motion throughout full treatment courses of stereotactic body radiotherapy for tumors in the liver.,” Acta Oncol. 52(7), 1437–44 (2013).

35 T. Ravkilde, P.J. Keall, K. Højbjerre, W. Fledelius, E. Worm, and P.R. Poulsen. “Geometric accuracy of dynamic MLC tracking with an implantable wired electromagnetic transponder”, Acta. Oncol. 50, 944-951 (2011).

36 S. Ipsen, R. Bruder, R.T. O’Brien, P.J. Keall, A. Schweikard, P.R. Poulsen. “Online 4D ultrasound guidance for real-time motion compensation by MLC tracking”, Med. Phys. 43, 5695-5704 (2016).

Figure captions

Figure 1: Polar plots of the first principal component vector showing the motion that occurs in the anterior-posterior and left-right direction when the tumor moves cranially for 99 lung tumor trajectories (left) and 695 prostate trajectories (right). The center of the polar plots corresponds to pure cranial motion. Each dot represents one trajectory. The yellow dot in the prostate figure is the global value used for prostate tracking with dynamic collimator rotation.

Figure 2: Examples of MLC exposure errors from MLC fitting to the target shift indicated by the red arrow without MLC tracking and with MLC tracking with the current TrueBeam MLC tracking system and MLC tracking system improvements (3)-(6) in Table 2.

Figure 3: Actual and predicted motion during two breathing cycles of a lung tumor trajectory.

Figure 4: 3D root-mean-square (RMS) prediction error (left) and mean residual MLC exposure error of MLC tracking relative to no tracking (middle: low modulation VMAT plan, right: high modulation VMAT plan) for the lung treatment simulations. Results are shown for trajectories with small (<5mm), medium (5-10mm) and large (>10mm) motion range as well as for all lung tumor trajectories.

Figure 5: 3D root-mean-square (RMS) prediction error (left) and mean residual MLC exposure error of MLC tracking relative to no tracking (middle: low modulation VMAT plan, right: high modulation VMAT plan) for the prostate treatment simulations. Results are shown for trajectories with motion ranges below and above 3mm as well as for all prostate trajectories.

Figure 6: Example of a prostate trajectory and the MLC exposure error as function of time during VMAT MLC tracking. (a): Prostate position in beam's eye view (BEV) perpendicular to the MLC leaves with the original 90° collimator rotation and with dynamic collimator rotation (Improvement (5) in Table 2). (b-c): MLC exposure error from the MLC leaf fitting step (b) and from all three MLC tracking steps combined (c) for the current MLC tracking system and improvements with Half leaf width (3), Jaw tracking (4) and Dynamic collimator rotation (5). The numbers indicate the mean MLC exposure error over the presented time interval.

Figure 7: Mean residual MLC exposure error compared with no tracking for tracking system improvements (1)-(7) and without improvements (0). The results are stratified by the motion range of the trajectories as indicated in the legends.

Figure 8: Mean MLC exposure error reduction relative to the current MLC tracking system with optimized prediction. All bars are normalized to the total mean MLC exposure error for the current system.

Table 1: The investigated prediction algorithms.

Name	Short name	Motivation
(a) No prediction	No prediction	Lower limit if no prediction is applied
(b) Linear Kalman filter	Kalman	Default algorithm for TrueBeam MLC tracking[17].
(c) Kernel density estimation[22]	KDE	Used in ongoing clinical study of lung MLC tracking on a Trilogy accelerator[28]
(d) Linear adaptive filtering[23]	LAF	Implemented in the clinically used Trilogy MLC tracking system.
(e) Wavelet-based multiscale auto regression[24]	wLMS	State-of-the-art. Best algorithm in comparative study with six prediction algorithms[29]
(f) Time-variant seasonal autoregressive[25]	TVSAR	State-of-the-art algorithm
(g) Perfect prediction	Perfect	Upper limit with optimal prediction algorithm

Table 2: Description of the seven MLC tracking system improvements

Name	Improvement
(1) No localization latency	No Calypso signal latency
(2) Fast MLC	MLC with doubled maximum speed, acceleration and de-acceleration
(3) Half leaf width	MLC with 2.5 mm leaf width instead of 5 mm
(4) Jaw tracking	Aperture edge defined by Y-jaws, open leaves at the aperture edge[12]
(5) Dynamic collimator rotation	Aligning collimator with the previously measured first principal component of tumor motion projected onto the collimator plane for each gantry angle[15]
(6) (4-5) combined	Combination of jaw tracking and dynamic collimator rotation
(7) (1-5) combined	Combination of all improvements

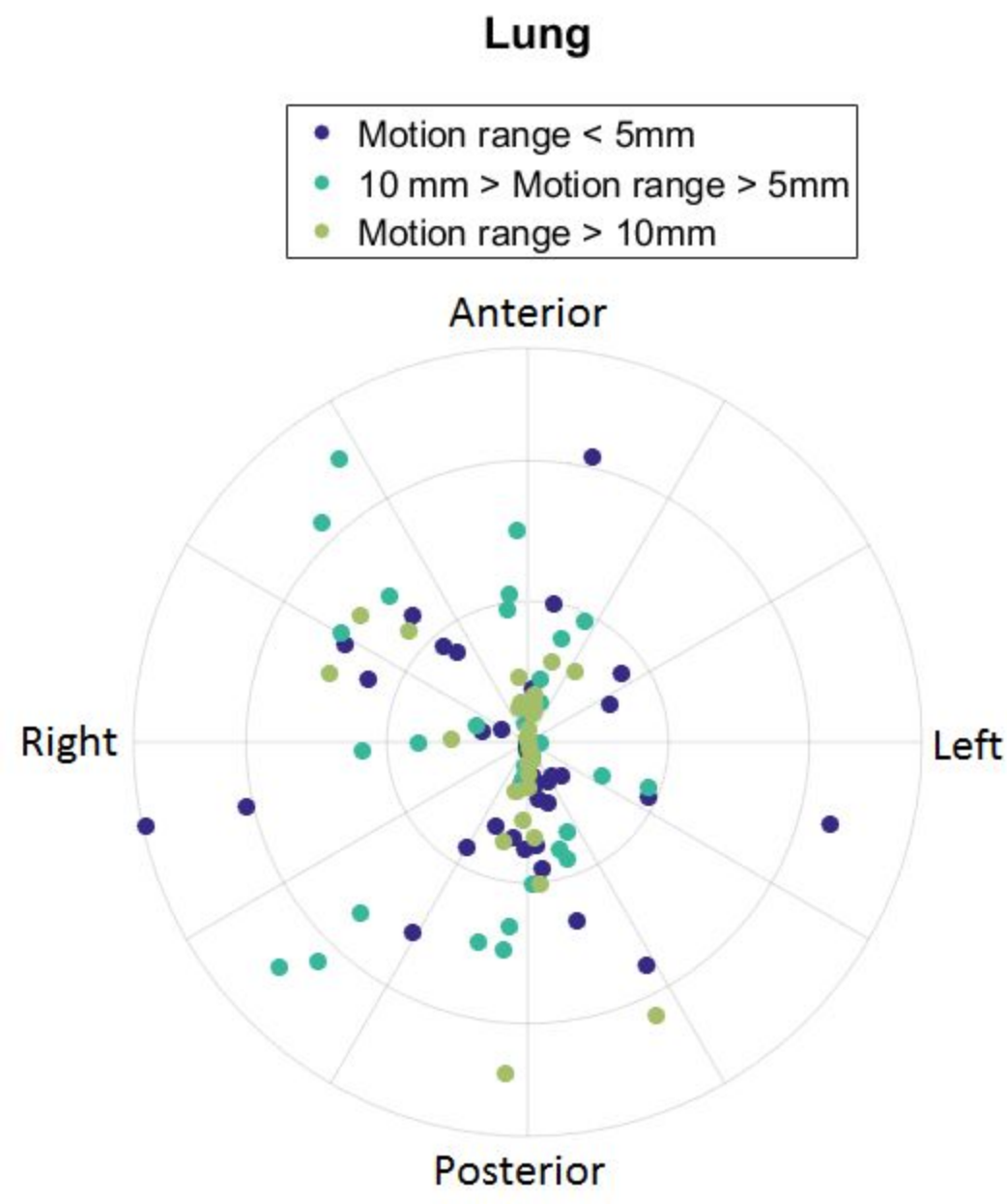
Lung
Motion range < 5mm
10 mm > Motion range > 5mm
Motion range > 10mm
Anterior
Right
Left
Posterior

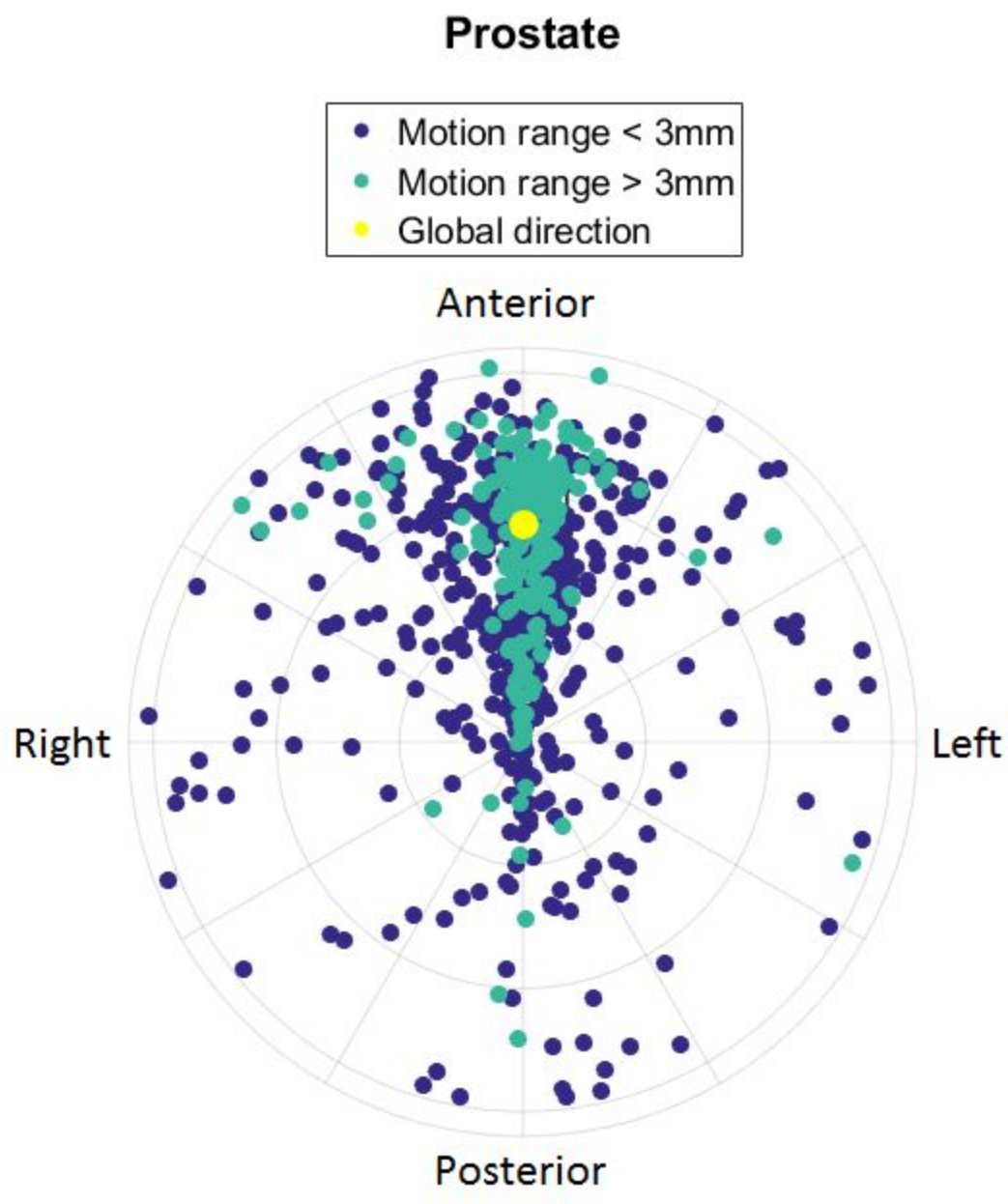
Prostate
Motion range < 3mm
Motion range > 3mm
Global direction
Anterior
Right
Left
Posterior

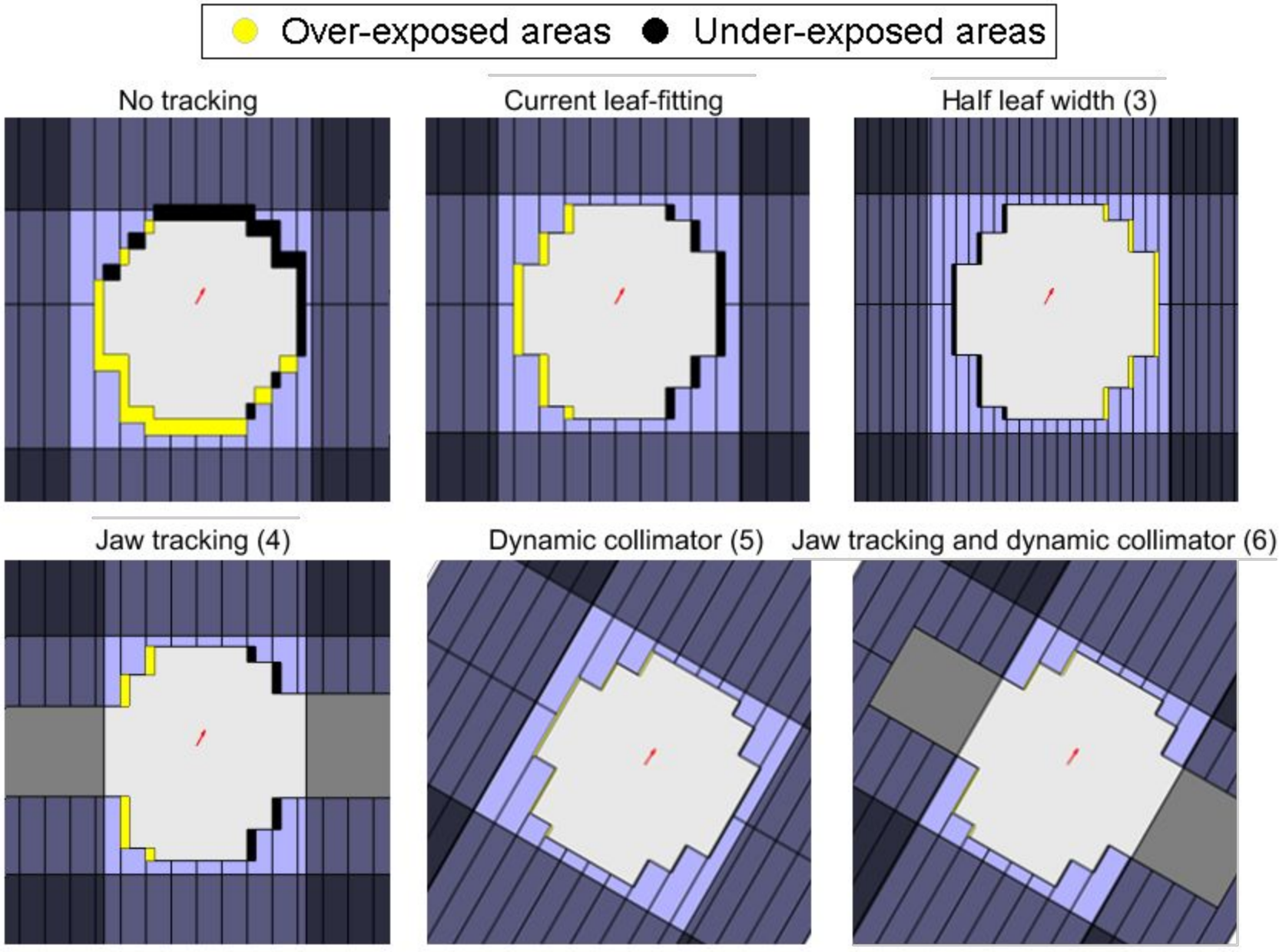
Over-exposed areas
Under-exposed areas
No tracking
Current leaf-fitting
Half leaf width (3)
Jaw tracking (4)
Dynamic collimator (5)
Jaw tracking and dynamic collimator (6)

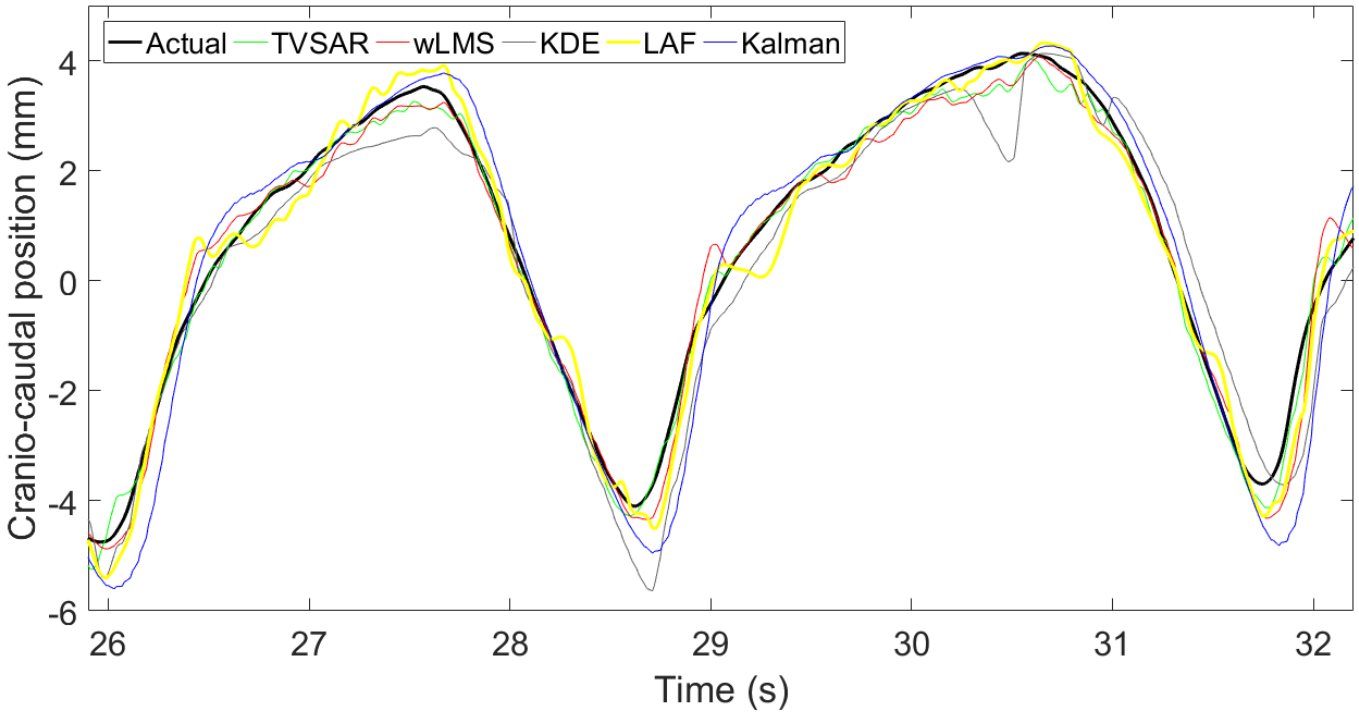
Actual
TVSAR
wLMS
KDE
LAF
Kalman
Cranio-caudal position (mm)
4
2
0
-2
-4
-6
26
27
28
29
30
31
32
Time (s)

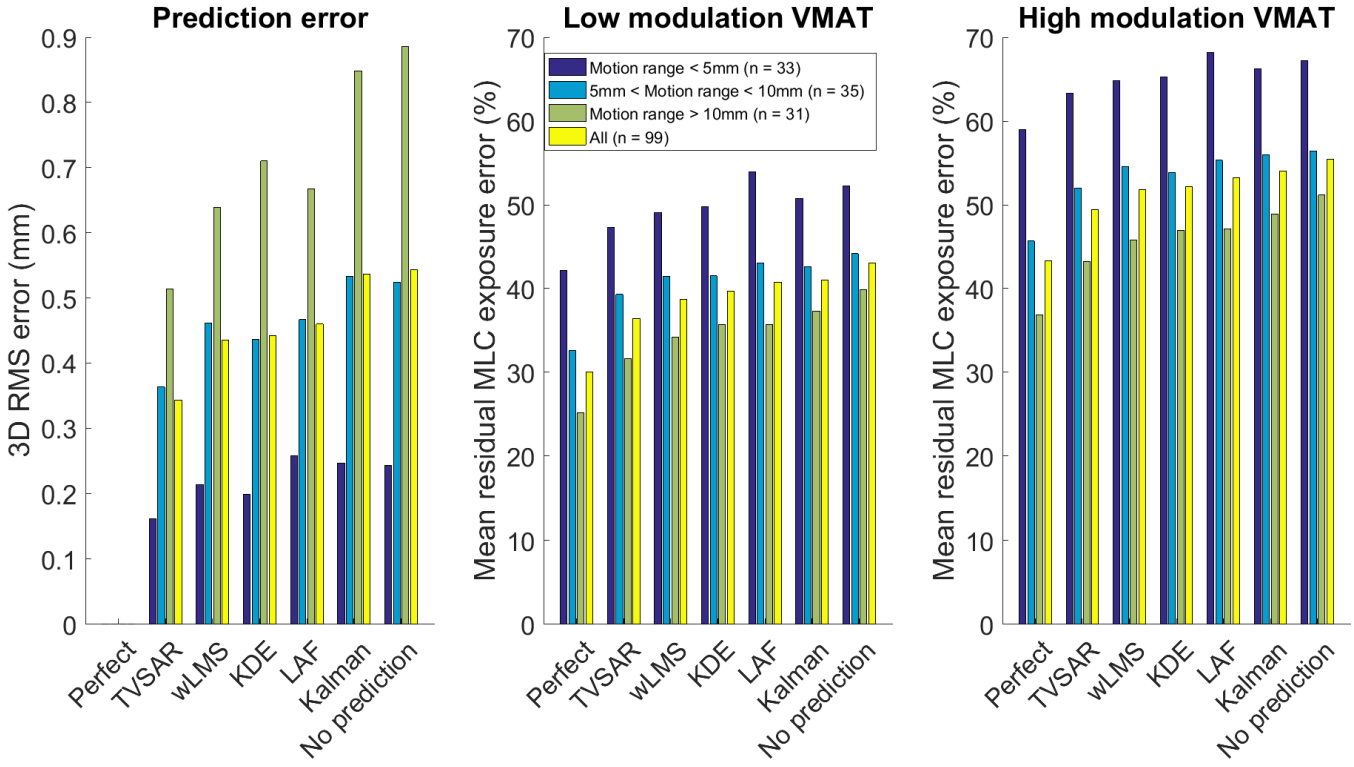
Prediction error
3D RMS error (mm)
0
0.1
0.2
0.3
0.4
0.5
0.6
0.7
0.8
0.9
Perfect
TVSAR
wLMS
KDE
LAF
Kalman
No prediction
Low modulation VMAT
Mean residual MLC exposure error (%)
0
10
20
30
40
50
60
70
Motion range < 5mm (n = 33)
5mm < Motion range < 10mm (n = 35)
Motion range > 10mm (n = 31)
All (n = 99)
Perfect
TVSAR
wLMS
KDE
LAF
Kalman
No prediction
High modulation VMAT
Mean residual MLC exposure error (%)
0
10
20
30
40
50
60
70
Perfect
TVSAR
wLMS
KDE
LAF
Kalman
No prediction

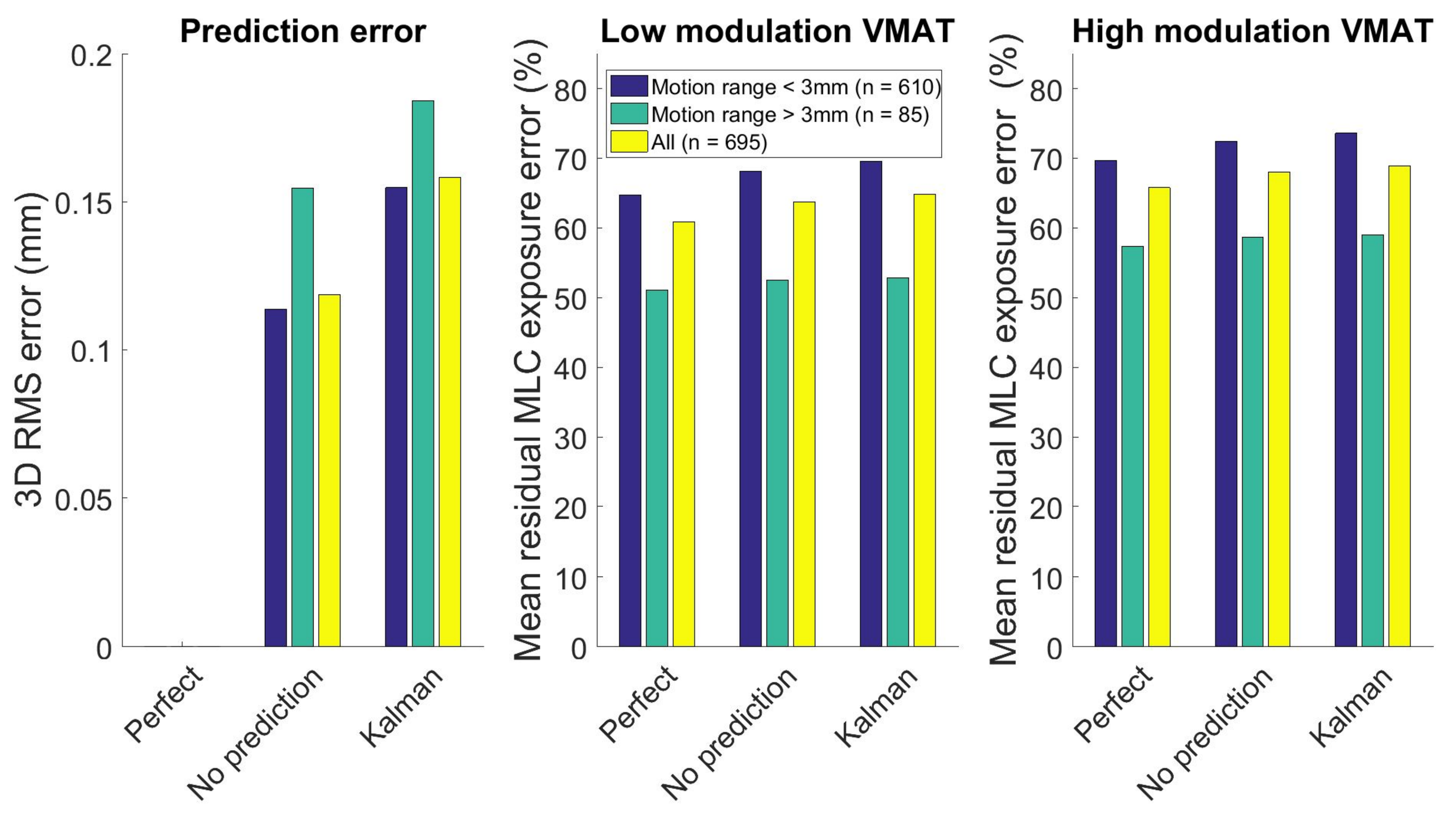
Prediction error
3D RMS error (mm)
0.2
0.15
0.1
0.05
0
Perfect
No prediction
Kalman
Low modulation VMAT
Mean residual MLC exposure error (%)
Motion range < 3mm (n = 610)
Motion range > 3mm (n = 85)
All (n = 695)
80
70
60
50
40
30
20
10
0
Perfect
No prediction
Kalman
High modulation VMAT
Mean residual MLC exposure error (%)
80
70
60
50
40
30
20
10
0
Perfect
No prediction
Kalman

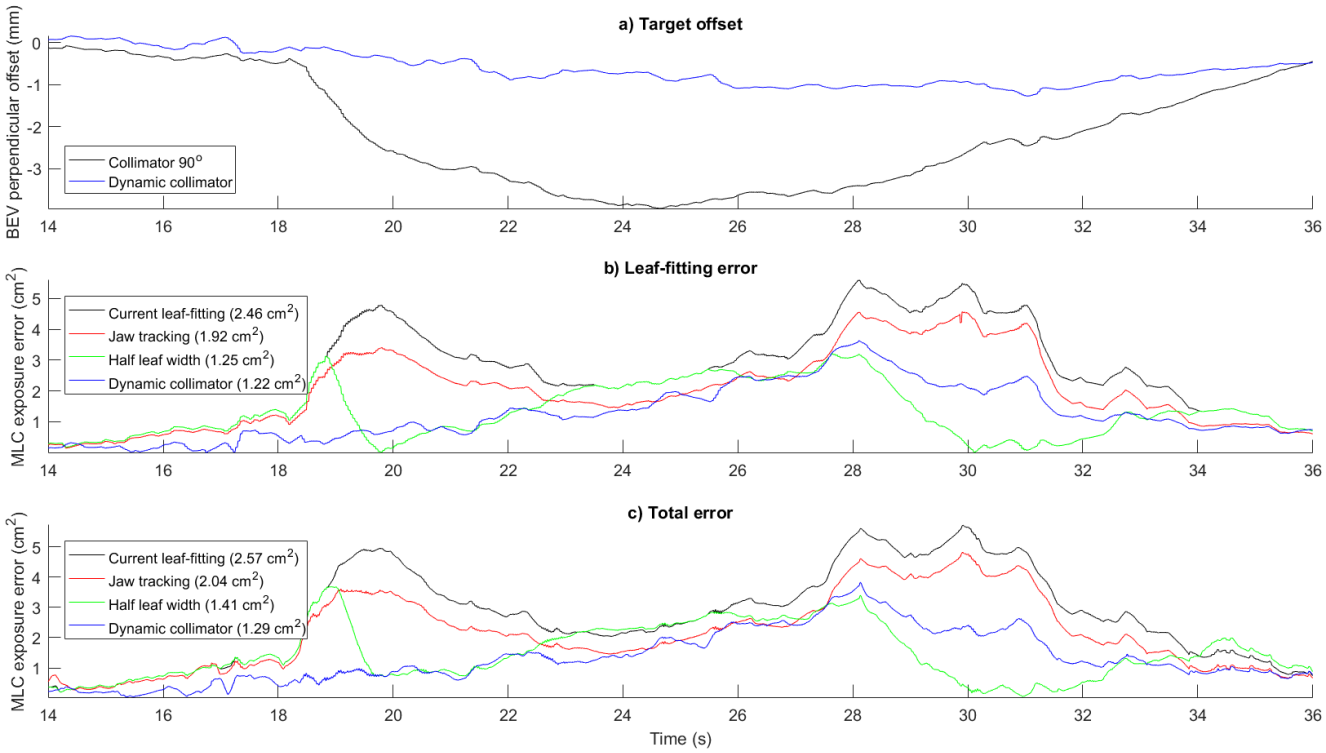
a) Target offset
BEV perpendicular offset (mm)
0
-1
-2
-3
Collimator 90°
Dynamic collimator
14
16
18
20
22
24
26
28
30
32
34
36
b) Leaf-fitting error
MLC exposure error (cm²)
Current leaf-fitting (2.46 cm²)
Jaw tracking (1.92 cm²)
Half leaf width (1.25 cm²)
Dynamic collimator (1.22 cm²)
c) Total error
Current leaf-fitting (2.57 cm²)
Jaw tracking (2.04 cm²)
Half leaf width (1.41 cm²)
Dynamic collimator (1.29 cm²)
Time (s)

Mean residual MLC exposure error (%)

Low modulation VMAT

High modulation VMAT

Lung

Prostate

0 mm < Motion range < 5mm (n = 33)
5mm < Motion range < 10mm (n = 35)
Motion range > 10mm (n = 31)
All (n = 99)

Motion range < 3mm (n = 610)
Motion range > 3mm (n = 85)
All (n = 695)

0
20
40
60
80
100

(0) (1) (2) (3) (4) (5) (6) (7)

Reference (0)
No localization latency (1)
Fast MLC (2)
Half leaf width (3)
Jaw tracking (JT) (4)
Dynamic collimator (DC) (5)
DC+JT (6)
All (7)

Mean MLC exposure error reduction (%)

Low modulation VMAT

High modulation VMAT

Lung

Prostate

Localization
Leaf-fitting
Leaf-adjustment
Total

60
40
20
0
-20

(1) (2) (3) (4) (5) (6) (7)

No localization latency (1)
Fast MLC (2)
Half leaf width (3)
Jaw tracking (JT) (4)
Dynamic collimator (DC) (5)
DC+JT (6)
All (7)